Evidence for a New Type of Shears Mechanism in ^{106}Cd

A. J. Simons, R. Wadsworth, and D. G. Jenkins
Department of Physics, University of York, Heslington, York Y010 5DD, United Kingdom

R. M. Clark, M. Cromaz, M. A. Deleplanque, R. M. Diamond, P. Fallon, G. J. Lane,* I. Y. Lee, A. O. Macchiavelli, F. S. Stephens, C. E. Svensson,† K. Vetter,‡ and D. Ward
Nuclear Science Division, Lawrence Berkeley National Laboratory, Berkeley, California 94720, USA

S. Frauendorf
Department of Physics, University of Notre Dame, Notre Dame, Indiana 46556, USA, and FZ Rossendorf, Postfach 510119, D-01314, Dresden, Germany
(Received 26 June 2003; published 14 October 2003)

Lifetimes of states in the lowest lying positive parity band in ^{106}Cd have been measured using the Doppler shift attenuation method. The deduced $B(E2)$ transition rates show a marked decrease with increasing spin. Cranking and semiclassical model calculations suggest that the structure has the character of a shears-type band resulting from the coupling of $g_{9/2}$ proton holes to aligned pairs of $h_{11/2}$ and $g_{7/2}$ neutron particles. This is the first clear evidence for the phenomenon of "antimagnetic" rotation in nuclei.

DOI: 10.1103/PhysRevLett.91.162501 PACS numbers: 21.10.Tg, 23.20.Lv, 25.70.Gh, 27.60.+j

Rotational bands in nuclei, consisting of strong electric quadrupole ($E2$) transitions, are most commonly interpreted as arising from the coherent collective rotation of many nucleons about an axis perpendicular to the symmetry axis [1]. For such nuclei, the density distribution is usually well deformed and this specifies the orientation in space in a manner similar to that observed in diatomic molecules. Over the past few years, a new type of rotational band, consisting of magnetic dipole ($M1$) transitions in nearly spherical nuclei, has been discovered in the light lead and cadmium/tin isotopes as well as other groups of nuclei (see [2,3]). The orientation of these rotors is specified by the current distribution of the high-j nucleons involved in the configurations rather than by their overall nuclear density distribution. This has been verified through lifetime measurements, which indicate that these structures have very small quadrupole deformation [4,5]. For these nuclei, the current loops of the valence nucleons break the isotropy as illustrated in Fig. 1(a). These loops generate a magnetic dipole vector that rotates and produces the strong $M1$ transitions. The name "magnetic rotation" (MR) was given to this phenomenon, which alludes to the fact that it is the current loops and the magnetic dipole that are rotating in space. The angular momentum vector of the valence proton particles is perpendicular to that resulting from the valence neutron holes at the band head (as proven by measurements of the g factor of the bandhead [6]). The resulting proton and neutron vectors form the blades of a pair of shears and the total angular momentum increases along the band by closing the blades of these shears. The existence of this "shears mechanism" [7] has been firmly established by measuring the $B(M1)$ values of the magnetic transitions, which decrease as the shears close and the transverse component of the magnetic dipole moment decreases. A detailed discussion of the phenomenon can be found in Refs. [2,3].

Figure 1(b) shows an alternative arrangement of high-j proton-hole and neutron-particle current loops, which also breaks the axial symmetry about the total angular momentum vector. This coupling can lead to a new kind of rotational band in near-spherical nuclei that has been termed "antimagnetic rotation" (AMR) [8]. This is because the configuration can also be considered as being composed of two "shears-like" subsystems (each consisting of one proton hole and one neutron particle in the example shown) of the magnetic type, the magnetic moments of which are antialigned. This is analogous with spin states in antiferromagnetism, where one-half of the atomic dipole moments are aligned on one sublattice, and the other half are aligned in the opposite direction on the

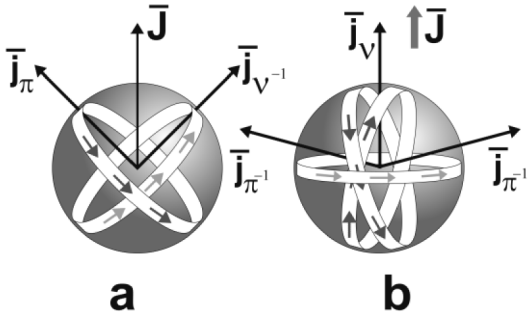

FIG. 1. Illustration of the shears mechanism for (a) magnetic and (b) antimagnetic cases. $\mathbf{J}$ is the total intrinsic angular momentum vector and $\mathbf{j}_\pi$ and $\mathbf{j}_\nu$ are the proton and neutron components, respectively. The vectors are not to scale. Both figures show the near-bandhead configuration for each mechanism.

 0031-9007/03/91(16)/162501(4)$20.00

second sublattice in crystalline cubic structures, thereby resulting in no net magnetic moment.

Antimagnetic rotation is expected to occur in the same regions, and under similar conditions, as magnetic rotation [2]; however, the best region is predicted to be in the light Cd isotopes. Here the two reorienting blades of the shears are formed from the angular momentum vectors of the same type of particle, i.e., two $g_{9/2}$ proton-hole blades [see Fig. 1(b)]. An increase in the total angular momentum is generated by the simultaneous closing of these two blades along the direction of the angular momentum vector of aligned neutron particles. Antimagnetic rotation differs from magnetic rotation in two important respects: (i) there is no net magnetic dipole moment because the individual moments cancel; (ii) the antimagnetic rotor is symmetric with respect to a rotation by π about the angular momentum axis. This implies that "antimagnetic bands" should consist of regular sequences of energy levels differing in spin by $2\hbar$ and that they should decay by weak $E2$ transitions, reflecting the weakly deformed core.

The phenomenon of antimagnetic rotation is characterized by a decrease of the $B(E2)$ values with increasing spin, which can be demonstrated by measuring lifetimes, and a large $\mathcal{J}^{(2)}/B(E2)$ ratio [$>100\ \mathrm{MeV}^{-1}\hbar^2(e\,\mathrm{b})^2$] [2], which increases with spin. Recently Zhu *et al.* [9] found the first evidence for the characteristic large $\mathcal{J}^{(2)}/B(E2)$ ratio in the light Pd isotopes. However, no lifetimes for individual states were measured. In this Letter, we report the results of an experiment to measure the lifetimes of states in the lowest lying positive parity band in ^{106}Cd [10]. The results provide the first conclusive evidence for this new type of shears mechanism in nuclei.

High-spin states in ^{106}Cd were populated using the ^{62}Ni(^{48}Ca, $4n$) reaction at beam energies of 183 and 207 MeV. The 183 MeV ^{48}Ca beam, accelerated by the 88-inch cyclotron at the Lawrence Berkeley National Laboratory, was incident on a target of 979 μg/cm^2 enriched ^{62}Ni on a backing of 18 mg/cm^2 of gold. The resulting γ decay was detected by the Gammasphere array [11], which contained 95 hyperpure Ge detectors. At the higher beam energy, a single thin ^{62}Ni foil of 520 μg/cm^2 was used as a target. A total of $\sim 2 \times 10^8$ events of threefold or higher coincidences were collected in the backed target data set, while $\sim 5 \times 10^8$ such events were obtained from the thin target experiment. The high-fold data were unfolded into triples events and sorted into γ-gated angle-dependent γ-γ correlation matrices.

Lifetimes were extracted by fitting the Doppler-broadened line shapes using the codes of Wells and Johnson [12]. The slowing down of recoiling nuclei in the target and gold backing was simulated using Monte Carlo methods with 5000 histories and a time step of 0.001 ps and treated according to the prescription of Gascon *et al.* [13]. The tables of Northcliffe and Schilling [14], with shell corrections, were used for the electronic stopping powers. The histories were used to reproduce velocity distributions for particular angular groups of detectors at an averaged angle based on the geometry of the Gammasphere array. Fits were carried out assuming a rotational cascade of five transitions, with a moment of inertia similar to that of the in-band transitions of $25\hbar^2\ \mathrm{MeV}^{-1}$, feeding into each state, including the topmost state. The side-feeding intensities were determined from the thin target data and compared with the values obtained in Ref. [10]. There was good agreement between the two sets of values. The main discrepancy was for the intensity feeding the 18^+ state, the value from Ref. [10] being 33% while that from the present work was 15%. The latter value was used in the present analysis.

Line shape parameters of transitions of interest and stopped contaminant peaks were simultaneously fitted to various combinations of spectra corresponding to detectors grouped at forward, backward, or transverse angles in Gammasphere. Typical line shape fits are shown in Fig. 2. The effective lifetime of the highest state observed was determined and used as an input parameter to a global fit of the entire cascade with variable lifetimes for both in-band and side-feeding states. An error analysis was performed by examining the behavior of the χ^2 value deduced for the fit in the vicinity of the minimum. The errors on the lifetimes were deduced from the uncertainty in the χ^2 minimization and from fitting each set of forward, backward, and transverse angles and the spread in the lifetime results obtained from each set of angles. The side-feeding lifetimes were found to be comparable to or up to 20% slower than the in-band lifetimes. The results of this analysis are presented in Table I. The errors included in the table do not account for systematic

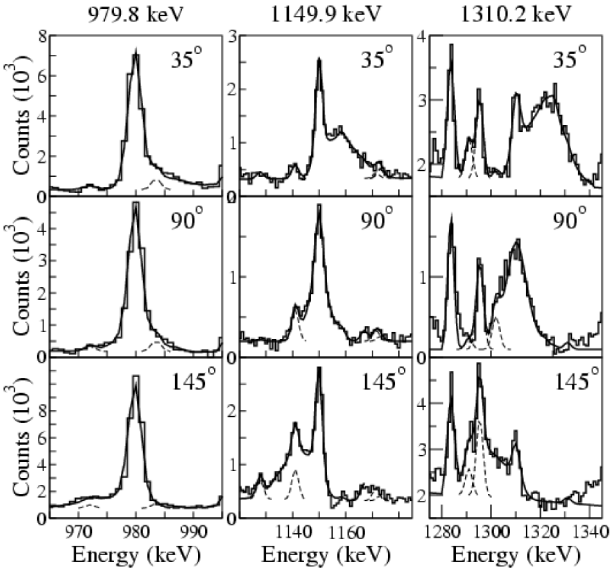

FIG. 2. Representative spectra and fitted line shapes (solid lines) for the 979.8, 1149.9, and 1310.2 keV γ rays in band 1 of ^{106}Cd. The dashed lines show contaminant peaks. The spectra shown are taken from averaged forward 31.72° and 37.34° ($\overline{\theta} = 34.57°$) rings (top), 90° ring (middle), and averaged backward 142.62° and 148.28° ($\overline{\theta} = 145.45°$) rings (bottom).

TABLE I. Lifetimes and deformations of ^{106}Cd. τ is the mean lifetime of the state, depopulated by the gamma ray, E_γ. Results are averaged from line shape fits to two sets of angles: ($\overline{35}°$, 90°, $\overline{145}°$), ($\overline{52}°$, 90°, $\overline{128}°$).The next two columns contain derived experimental quantities. The last column shows the calculated deformation parameter, ϵ_2.

$\mathbf{I_i}$	E_γ (keV)	τ (ps)	$B(E2)$ (e^2 b^2)	$\mathcal{J}^{(2)}/B(E2)$ (MeV^{-1}(e b)^2)	ϵ_2
18	980.8	$0.60^{+0.05}_{-0.05}$	$0.15^{+0.01}_{-0.01}$	158^{+11}_{-11}	0.16
20	1150.6	$0.29^{+0.04}_{-0.04}$	$0.14^{+0.02}_{-0.02}$	177^{+25}_{-25}	0.15
22	1310.6	$0.26^{+0.02}_{-0.02}$	$0.07^{+0.01}_{-0.01}$	274^{+39}_{-39}	0.12
24	1487.6	$0.19^{+0.02}_{-0.02}$	$0.05^{+0.01}_{-0.01}$	354^{+70}_{-70}	0.10

uncertainties such as the choice of stopping powers. Table I also shows values of $\mathcal{J}^{(2)}/B(E2)$, which clearly satisfy the criteron for antimagnetic rotation given earlier.

The thin target data were unfolded into triples events and sorted into an E_γ-E_γ-E_γ cube. These data were used to try to extend the band of interest, since previous work [10] had tentatively assigned an 1857.4 keV γ ray as feeding the 26^+ state. From the present data, no firm evidence could be found for this transition or any other γ rays decaying to the 26^+ level (see Fig. 3).

Previous work [10] assigned the $\nu[(h_{11/2})^2_{10}(g_{7/2})^2_6]$ configuration to band 1 above $J = 16$. This neutron configuration is represented by the vector $\vec{\mathbf{j}}_\nu$ in Fig. 1(b) and is coupled to the two $g_{9/2}$ proton holes, $\vec{\mathbf{j}}_{\pi^{-1}}$, whose angular momentum vectors are essentially perpendicular to the neutron angular momentum vector at $J \sim 16$.

Because of the symmetry of the antimagnetic configuration, the axis of rotation coincides with a principal axis. Accordingly, we have performed standard cranking calculations using Strutinsky renormalization in the absence of pairing. The energy of the $\nu(h_{11/2})^2(g_{7/2})^2$ configuration was minimized with respect to the deformation, ϵ_2, and triaxiality, γ, parameters for various angular momenta. Such calculations are often referred to as CNS calculations (e.g., see [2] for details). In the present work, we used the tilted axis cranking code (TAC) [2] because it allowed us to extract the relative orientation of the $g_{9/2}$ protons (see Fig. 3). Assuming zero pairing should be a good approximation due to the proximity of the $Z = 50$ proton shell gap and the presence of two pairs of aligned neutrons, thereby substantially reducing the pair correlations. The results indicate that the $g_{9/2}$ proton-hole spin vectors close rapidly as the spin increases above $J = 16$. At $\hbar\omega = 0.35$ ($J \approx 17$), the quadrupole deformation was found to be $\epsilon_2 = 0.158$ and $\gamma \approx 0°$, which agrees well with the results of the total Routhian surface (TRS) calculations reported in [10]. With increasing frequency, the triaxiality parameter, γ, remained close to 0° and there was a rapid decrease of ϵ_2, which becomes very small at $\hbar\omega = 0.65$ MeV ($J \approx 26$–28). This is in good agreement with the observed results (see Table I).

It is interesting to note that aligned pairs of $h_{11/2}$ and $g_{7/2}$ neutrons would be expected to yield a spin of $\sim 16\hbar$. If the alignment of a pair of $g_{9/2}$ proton-hole vectors was solely responsible for the resulting spin increase within this band beyond this point, the structure would be expected to terminate at spin $24\hbar$. (N.B. The Pauli principle prevents one of the two holes from reaching the maximal projection of $\frac{9}{2}\hbar$. Complete alignment corresponds to the projections $\frac{9}{2}\hbar + \frac{7}{2}\hbar = 8\hbar$.) The present results suggest that the deformed core contributes $\sim 2\hbar$ in the (16–26)$\hbar$ range. This is close to the cranking results, which indicate that nearly 70% of the spin within this range is generated by the shears mechanism.

Figure 3 demonstrates how the experimentally deduced and calculated $B(E2)$ values decrease with spin. The calculations are in reasonable agreement with the experimental data if the shape is optimized for each spin (full line) but cannot account for the data if a fixed deformation is assumed (dashed line). The observed rapid approach to a spherical shape reflects the shears mechanism. The neutron particles drive the core towards oblate deformation, while the proton holes are prolate driving. When the angular momenta of the protons and neutrons are aligned, their contributions tend to cancel, resulting

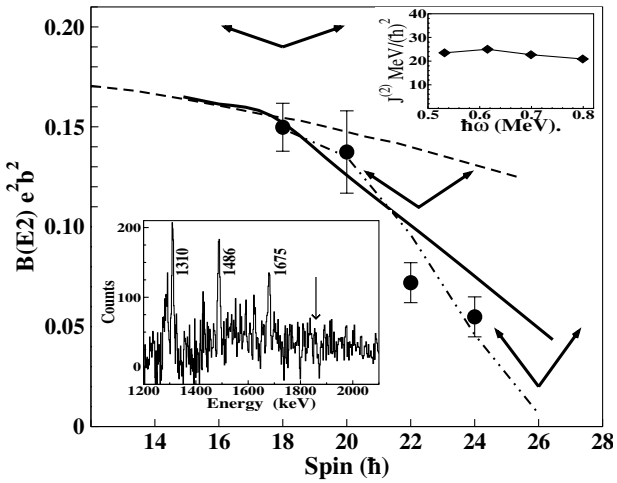

FIG. 3. $B(E2)$ values vs spin for band 1 in ^{106}Cd. The solid line shows the $B(E2)$ values calculated by optimizing the shape parameters ϵ_2 and γ as functions of the spin, whereas the dashed line displays them for constant $\epsilon_2 = 0.15$. The dot-dashed line depicts the semiclassical model assuming $j_\nu = 18$. The arrows show the relative orientation of the angular momentum of the $g_{9/2}$ proton holes. Insets: (top) Experimental $\mathcal{J}^{(2)}$ vs rotational frequency, (bottom) γ ray spectrum showing a sum of double gates from band 1 at 207 MeV. The arrow is located at the tentative γ ray discussed in [10].

in a near-spherical charge distribution and very small $B(E2)$ values. However, at the bandhead, when the angular momenta of the proton holes are perpendicular to the neutron angular momentum, they generate a small prolate deformation of the charge distribution, the symmetry axis of which is perpendicular to the rotational axis, yielding larger $B(E2)$ values. The calculation indicates that the proton holes resist the drive toward triaxiality, thereby leaving the nucleus with a near-axial shape. Thus, the closing of the shears is accompanied by a transition from a small prolate to almost zero deformation.

A semiclassical model description of the shears mechanism [3] yields a constant dynamic moment of inertia, $\mathcal{J}^{(2)}$, and a reduced transition probability of

$$B(E2) = \frac{15}{32\pi}(eQ_{\mathrm{eff}})^2\left[1 - \left(\frac{J - j_\nu}{2j_\pi}\right)^2\right]^2, \qquad (1)$$

where j_π and j_ν are the proton and neutron spin contributions, respectively, and J is the total spin. In [3], a value of $eQ_{\mathrm{eff}} = 6.5\ e\,\mathrm{b}$ was deduced for the magnetic shears bands in the $A \sim 198$ region. Scaling the mean square radius parameter given in [3] implies that, with a value of $eQ_{\mathrm{eff}} = 1\ e\,\mathrm{b}$, we require an effective proton charge $e_\pi \sim 1.3$, which agrees well with the previously deduced value for this mass region [15]. In the present calculation, we have taken $eQ_{\mathrm{eff}} = 1\ e\,\mathrm{b}$ and $j_\nu = 18$, which is consistent with the assumption that $\sim 2\hbar$ comes from the core contribution. Figure 3 shows that the model nicely reproduces the rapid decrease of the $B(E2)$ values. Overall, the semiclassical model appears to fit the data a little better than the TAC calculations.

As discussed earlier, the $\mathcal{J}^{(2)}/B(E2)$ ratio is expected to be large and to rise with increasing spin. This latter feature occurs because the $B(E2)$ values are small and decrease with increasing spin while the $\mathcal{J}^{(2)}$remains almost constant (see Fig. 3). These features can be derived within both the cranking and semiclassical models.

The collective rotation of well-deformed nuclei in the middle of a shell and the antimagnetic rotation of nuclei near closed shells are two extreme cases that can be clearly distinguished. However, when moving from one region to the other, the properties of the bands do not change abruptly and, consequently, the rotation may take an intermediate character. The group of nuclei which undergo "smooth band termination" are a salient example [16]. In a smoothly terminating band, the structure gradually develops from a prolate shape, rotating about an axis perpendicular to the symmetry axis, through a sequence of triaxial shapes to an oblate shape with the symmetry axis parallel to the total angular momentum vector. At this point, the angular momenta of the valence particles are fully aligned and the band terminates, just as the antimagnetic rotors terminate when the shears blades are aligned. However, the magnitude of the quadrupole deformation is larger than that expected for antimagnetic rotors, which start with a small deformation that is substantially reduced or even becomes zero when approaching termination. Moreover, the number of valence particles which generate the angular momentum increment in smoothly terminating bands (typically > 10 in the $A \sim 110$ region) is larger than for the antimagnetic rotors (2–6), which makes the rotation more collective.

In conclusion, lifetimes of states in the lowest lying positive parity band in ^{106}Cd have been studied using the Doppler shift attenuation method. The deduced $B(E2)$ values show a rapid decrease with increasing spin, which is in good agreement with both cranking and semiclassical model calculations. After the initial alignment of the $h_{11/2}$, $g_{7/2}$ neutrons at spin 16, the $g_{9/2}$ proton-hole vectors are almost antiparallel. As the spin increases, these vectors gradually close on the aligned neutron vectors and the spherical symmetry is restored. The present work indicates that much of the spin increase from $J = 16$–26 results from the antimagnetic form of the shears mechanism.

We thank the 88-Inch Cyclotron staff. This work was supported by the U.S. DoE, Contracts No. DE-AC03-76SF00098 and No. DE-FG02-95ER40934, and the U.K. EPSRC.

*Present address: Department of Nuclear Physics, Australian National University, Canberra, ACT 2000, Australia.
†Present address: Department of Physics, University of Guelph, Guelph, Ontario, Canada N1G 2W1.
‡Present address: Glenn T. Seaborg Institute, Lawrence Livermore National Laboratory, Livermore, CA 94550, USA.

[1] A. Bohr, Mat. Fys. Medd. K. Dan. Vidensk. Selsk. **26** (1952).
[2] S. Frauendorf, Rev. Mod. Phys. **73**, 463 (2001).
[3] R. M. Clark and A. O. Macchiavelli, Annu. Rev. Nucl. Part. Sci. **50** 1 (2000).
[4] R. M. Clark *et al.*, Phys. Rev. Lett. **82**, 3220 (1999).
[5] D. G. Jenkins *et al.*, Phys. Rev. Lett. **83**, 500 (1999).
[6] S. Chmel *et al.*, Phys. Rev. Lett. **79** 2002 (1997).
[7] G. Baldsiefen *et al.*, Nucl. Phys. **A574**, 521 (1994).
[8] S. Frauendorf, in *Proceedings of the Workshop on Gammasphere Physics, Berkeley* (World Scientific, Singapore, 1995), p. 272.
[9] S. Zhu *et al.*, Phys. Rev. C **64**, 041302 (2001).
[10] P. H. Regan *et al.*, Nucl. Phys. **A586**, 351 (1995).
[11] I. Y. Lee, Nucl. Phys. **A520**, 641c (1990).
[12] J. C. Wells and N. Johnson (private communication).
[13] J. Gascon *et al.*, Nucl. Phys. **A513**, 344 (1990).
[14] L. C. Northcliffe and R. F. Schilling, Nucl. Data Tables **7**, 233 (1970).
[15] M. Lipogalvsek *et al.*, Phys. Rev. Lett. **76**, 888 (1996).
[16] A. V. Afanasjev *et al.*, Phys. Rep. **322**, 1 (1999).